Geophys. J. Int. (2002) **148,** 77–87

A theoretical study of the effect of geomagnetic fluctuations and solar tides on the propagation of infrasonic waves in the upper atmosphere

Milton Garcés,[1] Douglas P. Drob[2] and J. Michael Picone[2]

[1] *Infrasound Laboratory,* 73–4460 *Queen Kaahumanu Hwy.,* 119, *Kailua-Kona,* HI 96740–2632. *E-mail: milton@isla.hawaii.edu*
[2] *Naval Research Laboratory, Washington, DC* 20375

Accepted 2001 August 3. Received 2001 July 31; in original form 1999 July 21

ABSTRACT

Propagating infrasonic waves are sensitive to changes in the atmospheric conditions. A theoretical acoustic wave propagation model is integrated with time-varying atmospheric models to investigate in more detail the effects of mesospheric and lower thermospheric variability on the propagation of infrasonic waves. We focus on the effects of the solar tides and geomagnetic perturbations on acoustic propagation in Alaska during winter of 1989–90, which corresponds to a period of solar maximum. Solar-driven tides are the strongest source of variability in mesospheric and lower thermospheric winds. These tides can alter the direction and magnitude of azimuth deviations, as well as the turning heights of ducted waves. Geomagnetic changes generally depress the turning heights of rays by increasing the thermospheric temperatures, and may either improve or deteriorate the azimuth deviations according to whether the geomagnetic-induced winds act with or against the tidal-induced winds. Observed arrivals with a low apparent horizontal phase velocity may be refracted in the thermosphere or the stratosphere. Unless the source epicentre and origin time are known, unambiguous phase identification can only be produced with knowledge of the stratospheric winds.

Key words: atmospheres, guided waves, infrasound, traveltime, wave propagation

INTRODUCTION

The Comprehensive Test Ban Treaty (CTBT) global infrasonic network of 60 arrays will permit the detection, identification and location of manifold natural and man-made events (McKisic 1997) from sources which may be thousands of kilometres away from recording sites. The characterization and precise location of these infrasonic sources will be determined by the accuracy of atmospheric state estimates that are utilized in infrasonic propagation models. Conversely, because of their high sensitivity to atmospheric conditions, continuous infrasonic measurements may improve or validate atmospheric models constructed from ground-based and satellite based atmospheric data sets. The atmosphere has various scales of variability at all heights; some of this variability is random and some is predictable. This theoretical manuscript is the first of a series of papers that will investigate the effects of deterministic atmospheric processes on the propagation of infrasonic waves in the atmosphere, with the aim of integrating ground measurements and theoretical predictions to improve source location accuracy. Throughout this manuscript, infrasonic waves refer to acoustic waves in the 0.02–5 Hz bandwidth of CTBT interest.

Infrasonic waves originating from a surface source may be ducted in four regions of the atmosphere (Fig. 1). In the troposphere, strong winds and boundary layer effects can trap infrasonic waves at low elevations. In the stratosphere, prevailing westerlies in the winter and easterlies in summer will produce strong returns along the dominant wind direction. The presence of these tropospheric and stratospheric ducts is dependent on the intensity and direction of the winds, and thus they may be sporadic or seasonal. However, if a source were placed in the low-velocity region between the upper troposphere and upper stratosphere ($\sim$10–40 km), it would be possible to trap acoustic energy in this region. Guided waves in this region would propagate with an apparent horizontal speed lower than the sound speed at the ground. Energy trapped in this mid-stratospheric duct may reach the ground through diffraction and scattering. A more detailed study of the tropospheric and stratospheric waveguides will be presented in a separate study. This manuscript concentrates on the propagation of sound waves in the lower thermosphere.

The high temperature gradient of the thermosphere will consistently refract infrasonic waves back to the ground in at least two distinct regions. Following the nomenclature of Brown

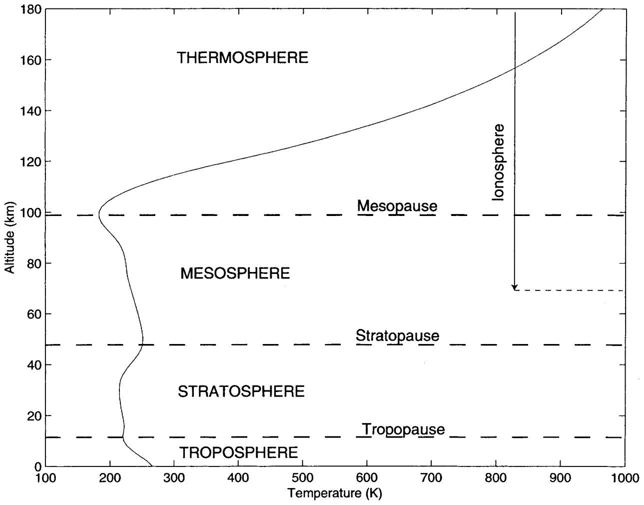

Figure 1. Temperature profile for a typical winter day in Alaska. Acoustic waveguides may be generated in the troposphere and stratosphere by strong winds. Waves propagating upwards are refracted back to the ground by the sharp increase in temperature in the thermosphere.

(1999), infrasonic arrivals corresponding to refraction in the troposphere, stratosphere, and thermosphere are referred to as Iw, Is, and It phases, respectively. Thermospheric refraction below and above 120 km may produce bifurcations in travel-time curves (Garcés *et al.* 1998). These branches are referred to as Ita (lower level refraction) and Itb (upper level refraction). Thermospheric arrivals, in particular Itb arrivals, may have relatively small amplitudes and longer periods, as the high frequency components of these thermospheric returns may be strongly attenuated by viscous and thermal losses in the highly rarefied gas of the diffusive region above 100 km (McKisic 1997). However, thermospheric phases will be valuable for infrasonic tracking of severe weather and for the interpretation of acoustic energy radiated by high altitude sources, such as rockets.

The temperature, composition and wind profiles in the atmosphere produce an acoustic propagation medium which is anisotropic and inhomogeneous. As sound waves propagate through the atmosphere, the wind component transverse to the wave normal causes a drift in the wave packet, so that its apparent arrival direction may not correspond to the original launch direction. The angular measure between the true source bearing and the observed source bearing is known as the azimuth deviation. Both the troposphere and stratosphere are relatively unaffected by tidal, extreme ultraviolet (EUV) and geomagnetic forcing. In contrast, the rarefied gas in the mesosphere and lower thermosphere responds strongly to tidal effects and the charged gas of the ionosphere is quite sensitive to geomagnetic and EUV forcing. Due to extreme acoustic attenuation above 150 km, we are only concerned with sound propagation below this region.

Early studies of atmospheric effects on infrasonic waves (Donn & Rind 1971; Rind & Donn 1975; Georges & Beasley 1977) were limited by the lack of detailed upper atmospheric data and reference models. Georges & Beasley (1977) traced rays through summer and winter atmospheric models, and noted that different azimuth deviations may be observed for different phases. However, due to their choice of propagation models, they predicted relatively large azimuth deviations. In contrast, historical data sets report relatively small azimuth deviations (Whitaker & ReVelle, personal communication, 1999). Our results confirm the reported small azimuth deviations, with the notable exception of ltb phases that penetrate into the thermosphere during strong tidal-induced winds. Donn & Rind (1971) interpreted four years of microbarom signals associated with severe weather in the North Atlantic. They observed a semidiurnal variation in microbarom amplitudes, which they attributed to semidiurnal changes induced by solar-driven tides. Their observations demonstrate that infrasonic signals are sensitive to fine-scale changes in the upper atmosphere. Thus, auscultation of severe weather patterns continuously present in the word's oceans may provide a useful tool for monitoring and updating upper atmosphere meteorological models.

Significant improvements in our understanding of the middle and upper atmosphere have occurred over the last 20 years. The results presented herein show detailed calculations of the effects on infrasound propagation of tidal and geomagnetic forcing of the atmosphere. In this study we use the MSISE-90 and HWM-93 empirical reference models (Hedin 1991; Hedin *et al.* 1994, 1996) which include detailed parametrizations of the dominant solar migrating tides, geomagnetic and solar forcing effects, low-order stationary planetary waves, and seasonal changes in the mean state. These models include only minor variability in the stratosphere, therefore in this study we concentrate on processes that predominantly affect the upper Mesosphere and Lower Thermosphere (henceforth referred to as the MLT). To further focus our study we will only consider the season of winter, when we have relatively steady stratospheric winds and the Earth is closest to the Sun.

SOURCES OF MLT VARIABILITY

The solar Westward-migrating tides are one of the largest sources of variability in the MLT region. Unlike lunar gravitational tides, these tides are the result of the daily periodic solar heating of water vapour in the troposphere, ozone in the stratosphere, and O_2 and N_2 in the lower thermosphere. These forced modes of oscillation travel westward with the apparent motion of the Sun and have periods of 24, 12 and 8 hr which are fixed in local time. These tides also propagate vertically and couple the lower atmosphere and the MLT region. The resulting tidal perturbations exhibit a strong latitudinal dependence, as they must satisfy the eigenmode solutions of forced fluid oscillations on a sphere (Andrews *et al.* 1987). Furthermore, these tides exhibit a strong seasonal pattern because their forcing depends on the amounts of troposphere water vapour, stratospheric ozone and available solar insulation, which vary as a function of season (Forbes 1999). The dominant modes of the migrating solar tides are parametrized in the MSISE-90 and HWM-93 model using spherical and vector spherical harmonics that have been modulated as a function of season using Fourier harmonics in day-of-year. Amplitudes and phases have been determined by fitting these harmonics to a long-term multi-instrument database of wind and temperature observations.

Geomagnetic storms are another important source of upper atmospheric variability with the potential to affect infrasound propagation in the MLT region. These effects are accentuated in the high-latitude ionosphere, where electromagnetic perturbations drive large changes in the MLT winds and temperatures though enhanced auroral particle precipitation and ion-neutral coupling processes (e.g. Salah *et al.* 1996; Prolss 1997). These geomagnetic storms, which perturb the atmosphere over many length and time scales, are also a natural source of infrasonic waves (Procunier 1971; Wilson *et al.* 1996). Geomagnetic activity is closely associated to solar flare activity and is monitored globally using several geomagnetic activity indices (e.g. Kp, Ap, Dst). The MSISE-90 and HWM-93 models uses a time history of Ap indices to parametrize the wind and temperature responses to geomagnetic activity perturbations.

Solar EUV radiation also plays a role in determining the structure and variability of the lower thermosphere. Solar EUV flux is the dominant energy source the atmosphere above 100 km where it is absorbed by O, O_2, and N_2 (e.g. Roble 1995). Solar EUV flux can vary by a factor of 4 over the 11 year solar cycle causing upper thermospheric temperatures to range from 700 to 1500 K through the cycle. The solar EUV flux also varies significantly at periods of near 27 days due to solar rotation. While the majority of this energy is deposited at 100–200 km heights, EUV flux can effect temperatures in the MLT directly and indirectly though downward conduction. Ground-based measurement of 10.7 cm radio flux, commonly referred to as the $F_{10.7}$ index, provides a convenient proxy for solar EUV flux (Hitteregger 1981). The $F_{10.7}$ index is used in the MSISE-90 and HWM-93 models to parametrize observed wind and temperature responses.

ATMOSPHERIC AND ACOUSTIC PROPAGATION MODELS

To trace rays in the atmosphere, it is necessary to have detailed knowledge of the sound speed and winds in the atmosphere (Garcés *et al.* 1998). The sound speed, c, is evaluated from the ideal gas law and the adiabatic equation,

$$c = \sqrt{\frac{\gamma R T}{m}} \tag{1}$$

where γ is the ratio of the heat capacities, R is the gas constant, m is the molecular mass, and T is the temperature in Kelvin. As discussed above, we use the Mass Spectrometer Incoherent Scatter (MSISE-90) and Horizontal Wind (HWM-93) models in this study to provide estimates of winds, temperature and molecular mass over the globe from the ground up to the upper thermosphere. The atmospheric models, accurate to first order, provide all the information needed to trace rays in the atmosphere.

To illustrate the effects of geomagnetic fluctuations and solar tides in infrasound propagation, we examine in detail the atmospheric conditions over Eielson, Alaska, for the solar maximum year of 1989. Climatologies for Eielson, AK (64.8 N, 146.9 W) were evaluated every three hours for 90 days of winter, from November 1 to January 31, 1989–1990. Profiles for the temperature, molecular mass, and zonal and meridional winds

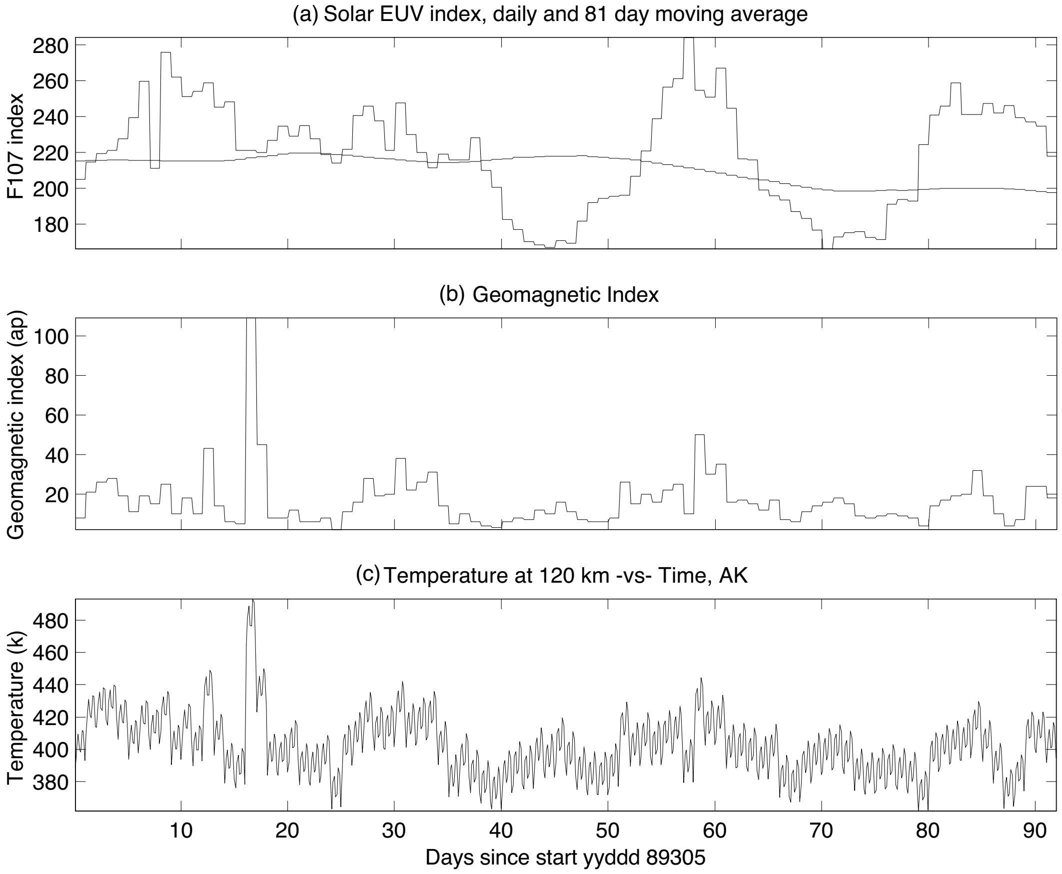

Figure 2. Solar F10.7 EUV index, geomagnetic AP index, and temperature (K) at 120 km as a function of winter day number, starting on November 1, 1989. An increase of the AP index increases the temperature of the lower thermosphere, and also induces a wind component that may counter the tidal winds. Note the peak in the AP index and the 120 km temperature corresponding to a geomagnetic storm on day 17.

were evaluated every two kilometres from the ground up to 180 km. Fig. 2(a) shows the $F_{10.7}$ index and the geomagnetic AP index for the season of winter 1989–90. Although the high $F10_{.7}$ index increases the thermospheric temperature, thus encouraging rays to turn at a lower level, the fine structure of the variability seen in Fig. 2(a) did not produce a significant change in infrasonic wave propagation. It is likely that this is because changes in EUV flux do not significantly effect the global scale wind patterns at these altitudes. The effects of EUV flux variability on the magnitude of the diurnal and semi-diurnal tides at MLT altitudes, however, is likely to be significant but is not parametrized in the current empirical models.

In contrast geomagnetic activity (Fig. 2b) can produce significant transient effects in the lower thermosphere, especially at high latitudes. The third panel of Fig. 2(c) shows the thermospheric temperature at 120 km as parametrized by the MSISE-90 model. It is evident that the temperature increases with increased geomagnetic activity due to the deposition of energy from enhanced high-latitude auroral precipitation. The geomagnetic storm on winter day 17 should be noted, as its effects can be clearly observed in the model output.

Fig. 3 shows the sound speed as a function of day number, height and time of day. The increase in sound speed in the stratopause is relatively weak compared to the drastic increase in the thermosphere. Diurnal fluctuations in sound speed near the stratopause will be fairly small in comparison with tidal-induced wind fluctuations in the upper atmosphere. This is convenient, as it is important to recognise whether propagation effects are due to temperature or wind variability.The MSISE empirical model produces upper atmosphere sound speed profiles that are fairly stable through the day. However, the winds may vary significantly, as shown in Figs 4 and 5. Fig. 4 shows meridional wind velocity, positive towards the North, as a function of height, day number and time of day. The dominant sources of variability are solar tides in the mesosphere and geomagnetic fluctuations in the thermosphere. The diurnal component of the solar tide is dominant above 150 km and the semidiurnal component of the tide dominates near 120 km at this latitude. Of particular interest is the high Northward wind velocity above 150 km at 9 h local time. At 18 h local time, when the thermospheric tidal wind is relatively weak, it may be reversed by winds induced by geomagnetic storms. Fig. 5 shows the zonal winds (positive towards the East), which have similar trends as those discussed in Fig. 4, except the times when geomagnetic storms may reverse the tidal wind (0 h and 3 h). The winter stratospheric wind at Alaska is quite stable in the models, and directed towards the southeast. The stratospheric models used in this study represent only nine year

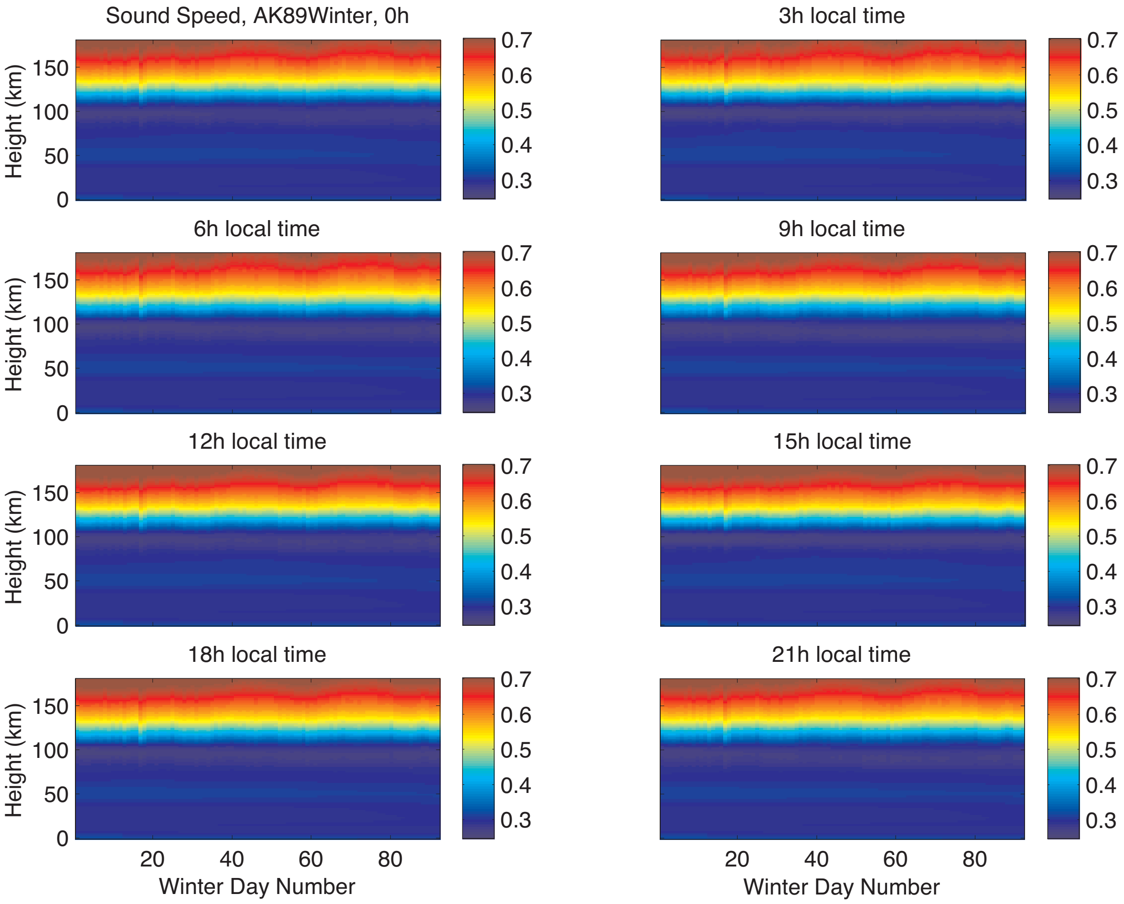

Figure 3. Sound speed in km s $^{-1}$, as a function of height, local time in hours and winter day number. There is a small increase in the sound speed near 50 km, and a drastic increase in the sound speed above the thermosphere, where the temperature increases rapidly and the molecular weight decreases with increasing height. The sound speed in the thermosphere is increased by heating during geomagnetic storms. However, compared to the winds, the sound speed is relatively stable through the season.

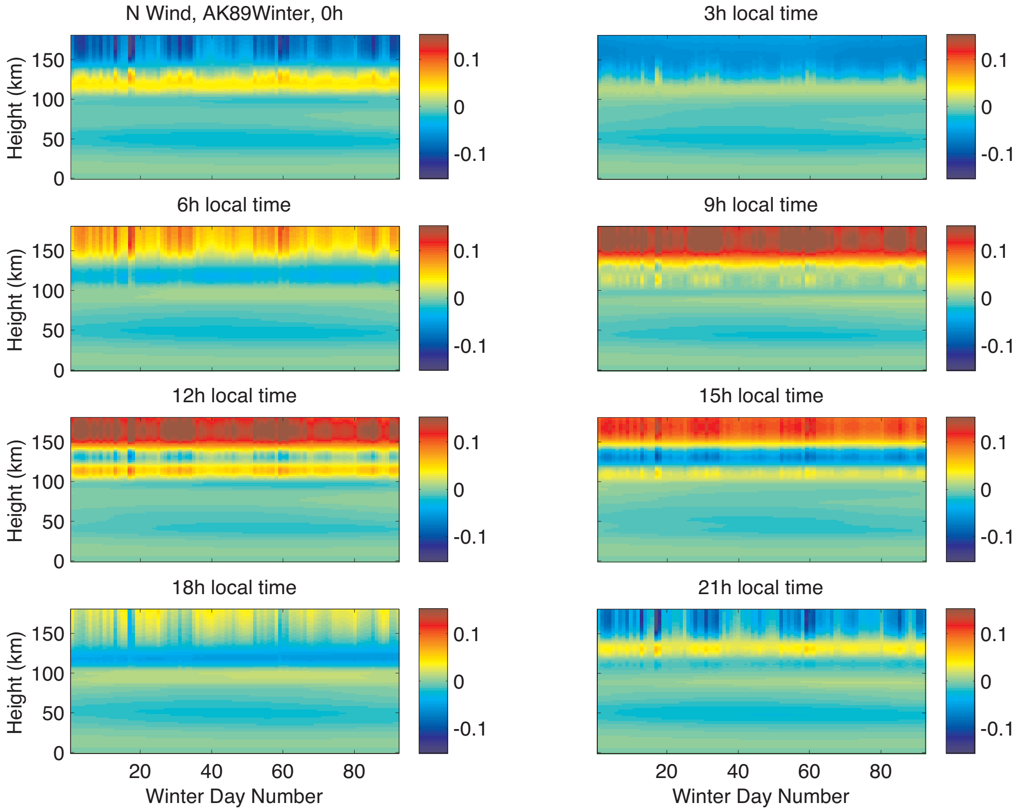

Figure 4. Meridional wind component in km s $^{-1}$, positive towards the north, as a function of height, local time and winter day number. The semidiurnal component of the tide is dominant near 120 km, and the diurnal component of the tide predominates above 140 km. Note the high thermospheric wind speed at 9h and 12h. Winds induced by geomagnetic storms may reverse the tidal winds.

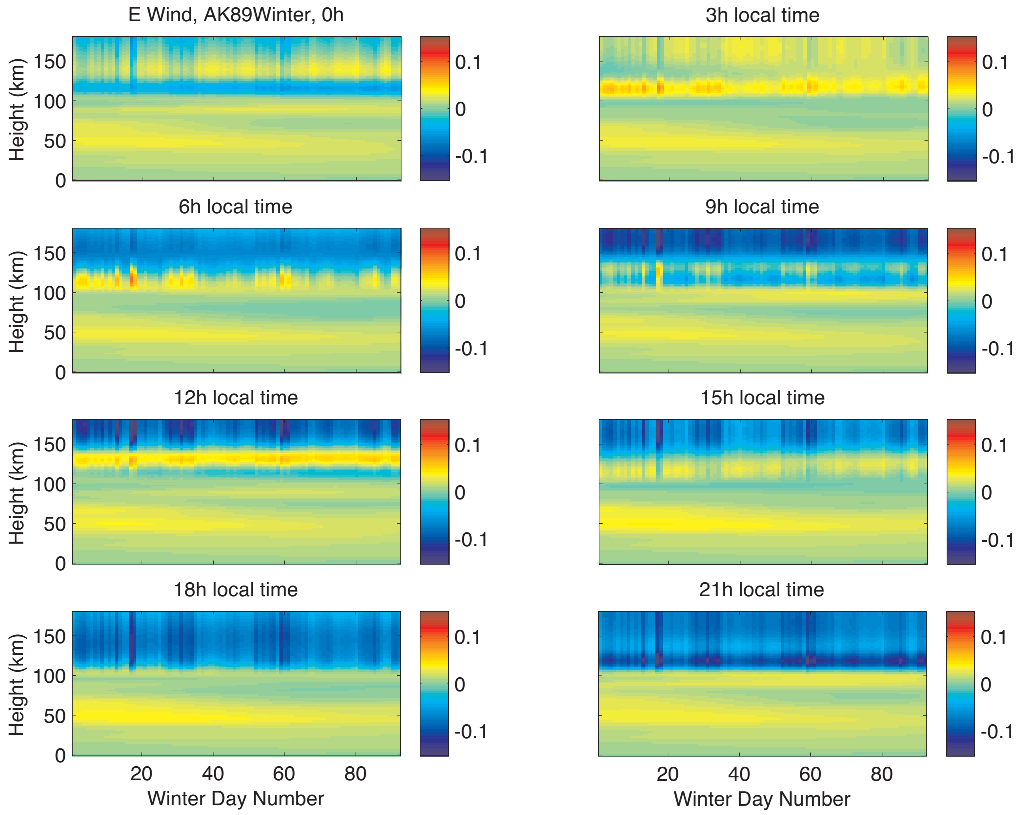

Figure 5. Zonal wind component in km s $^{-1}$, positive towards the east. Prominent features of the zonal winds are similar to those of Fig. 4, but less pronounced.

climatological averages of slowly varying stationary planetary waves. The effects of non-stationary planetary waves are important, and will be the subject of a separate study.

The infrasound propagation model of Garcés *et al.* (1998) is used to evaluate traveltime and azimuth deviation information. We assume a surface source and launch 50 rays in the four cardinal directions, considering only the first ground arrival. We then discuss the rays propagating towards the east and west, corresponding to downstream and upstream propagation with respect to the stratospheric winds. In addition, the strong meridional winds should produce the largest azimuth deviations allowed by the models. Comparable effects are observed for north–south propagation, but trends and phases are clearer in the east–west propagation directions.

MODEL RESULTS

We launch 50 rays towards the east, using the atmospheric profiles shown in Figs 3–5. Fig. 6 shows traveltime as a function of range and local time. Each curve represents a superposition of traveltime curves for all days of winter at that specific hour. Three distinct branches can be clearly identified in Fig. 6: one corresponding to stratospheric refraction (Is) and two corresponding to thermospheric refraction (Ita and Itb). Fig. 7 shows the turning heights as a function of slowness, winter day, and local time. The Is phases have a clear turning height near 40 km, and correspond to fairly narrow family of high slowness rays—rays with a shallow launch angle. The width of the region indicates how much of the total radiated acoustic energy is trapped by the stratospheric duct. As can be seen in Fig. 7, a small fraction of its total energy from an isotropic source will go into the Is phase. However, it may be possible to scatter some of the steeper rays into the stratospheric waveguide. Since this phase will have the least attenuation, when present it may have the highest amplitude. Most of the source energy that is not lost to space goes to the It phases, but due to enhanced attenuation, they may have lower amplitudes and be stripped of high-frequency energy. Fig. 7 shows that acoustic energy may be widely distributed over the mesosphere and lower thermosphere, but that at certain times of the day the solar tides may produce well-defined turning heights. Specifically, at 6 h and 15 h local time we can see two well-defined turning point regions in the thermosphere near 120 km (Ita) and above 150 km (Itb). The higher the turning point, the better defined phase Itb becomes in traveltime plots, as shown in Fig. 6. Also note that the range where the first arriving thermospheric phase may be observed varies through the day.

Fig. 8 shows the azimuth deviations for eastward propagation as a function of range and local time, where each curve shows a superposition of all traveltime curves for winter, as in Fig. 6. Fig. 9 shows deviations as a function of ray parameter, day number and local time. Positive deviations, in degrees, are to the right of the direction of propagation. Both Is and Ita phases

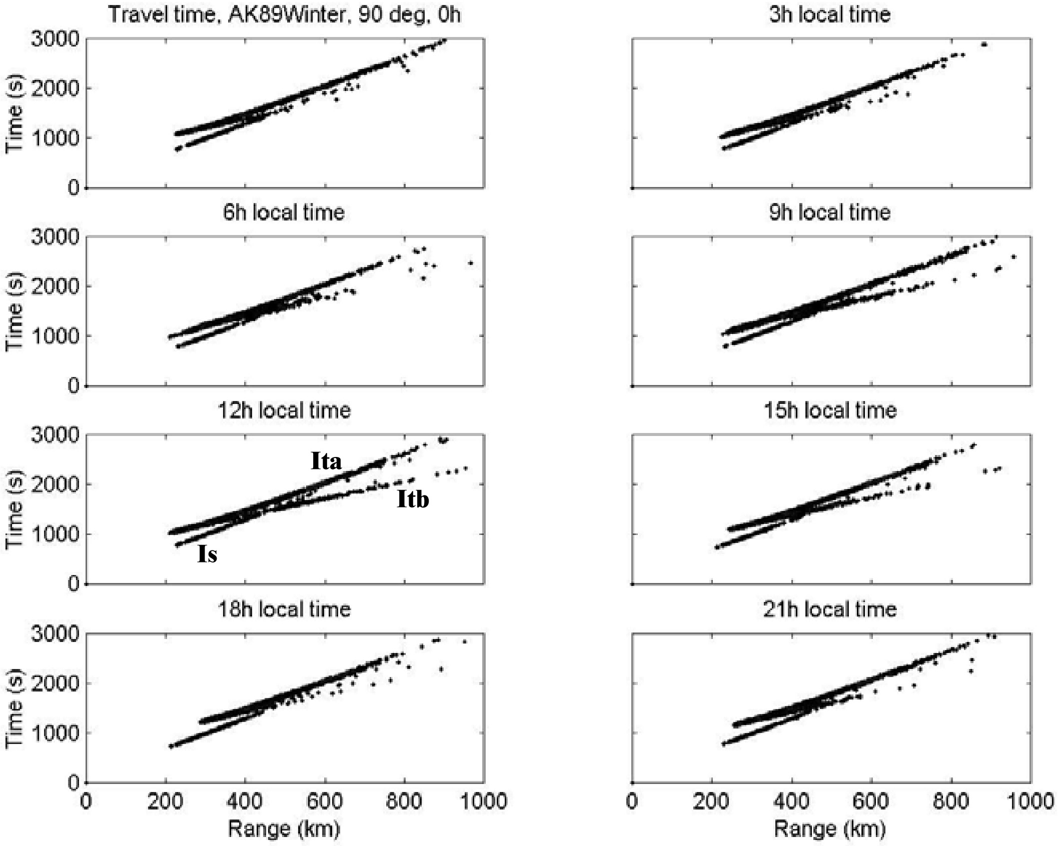

Figure 6. Traveltime curves for infrasonic waves propagating towards the east. All the traveltime curves for the season of winter are superposed. Each line corresponds to a distinct phase and to different reflection levels in the atmosphere. The stratospheric phase arrives at the earliest possible time, but at certain times of the day the extent of its shadow zone may be comparable to that of the thermospheric phase.

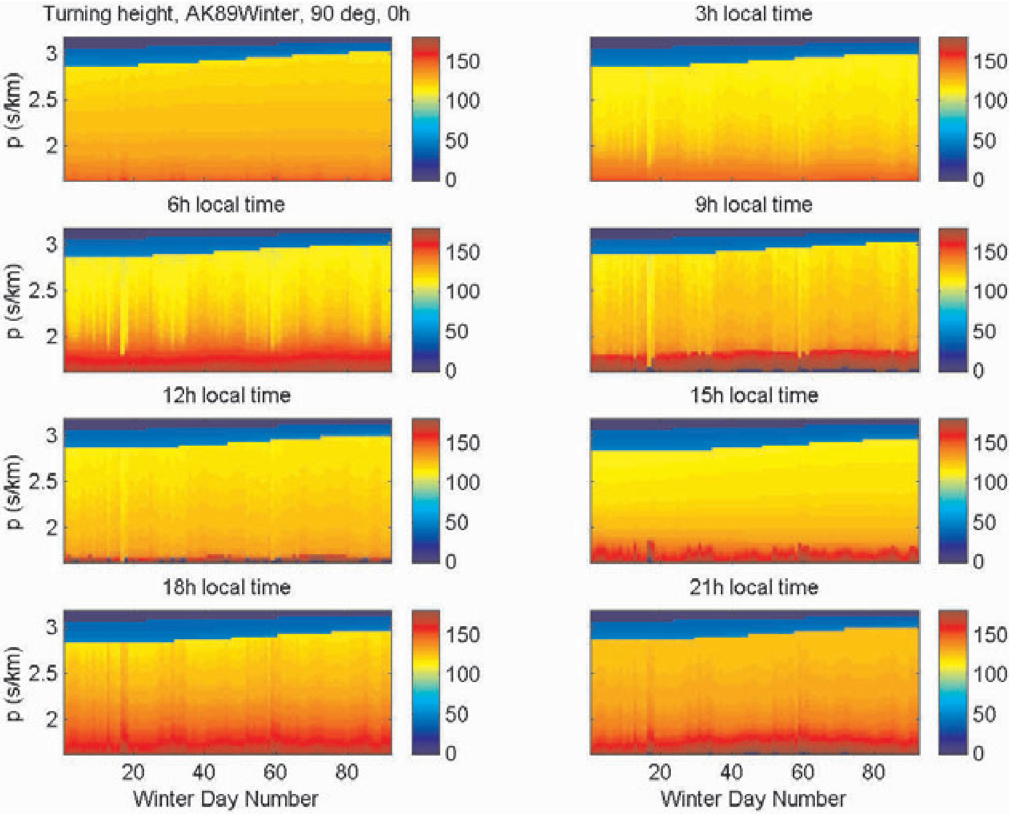

Figure 7. Turning heights for eastward propagation. The stratospheric phases have a clearly defined turning point near 50 km. The height ranges corresponding to the two thermospheric phases depend on tidal winds.

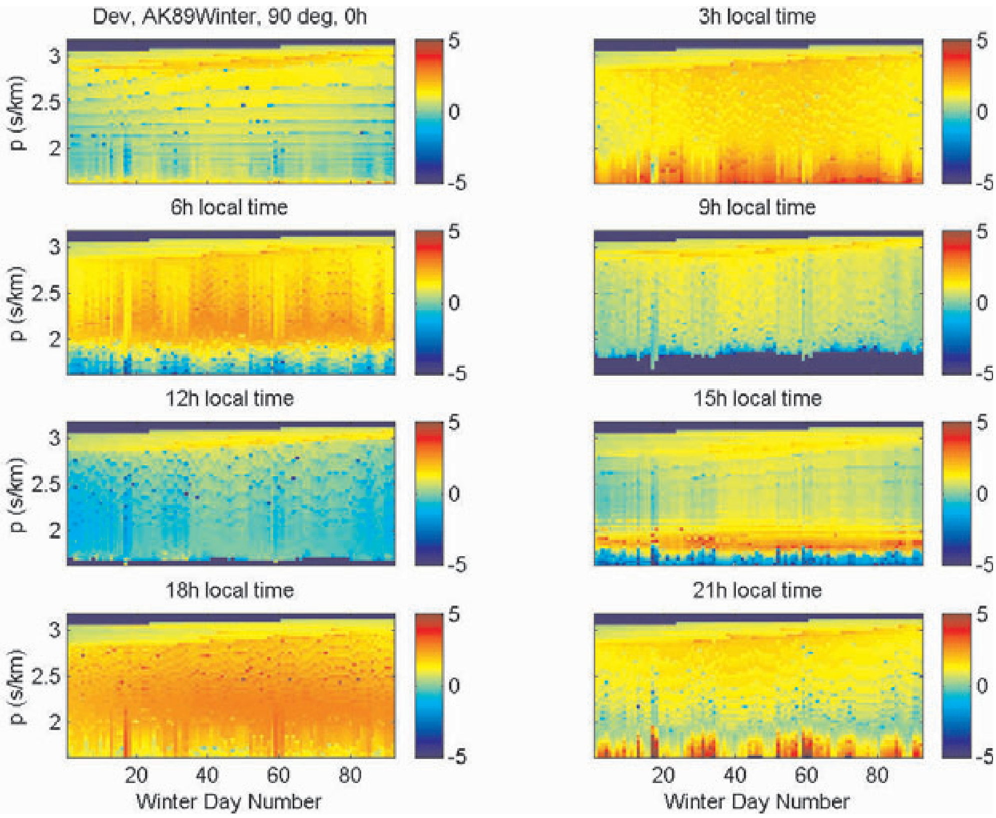

Figure 9. Azimuth deviation for eastward propagation as a function slowness, local time and winter day number. The steepest rays (lowest slowness) have the largest deviations and stratospheric phases have small deviations.

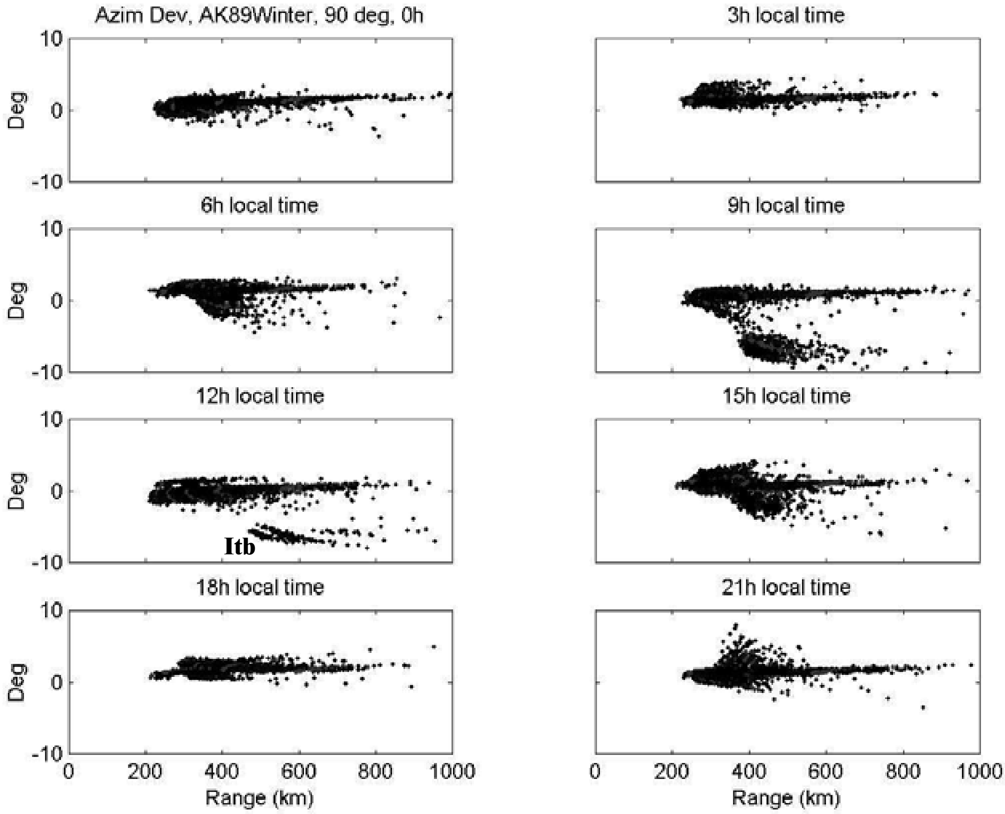

Figure 8. Azimuth deviation as a function of range and local hour for infrasonic waves propagating towards the east. All the azimuth deviations for the season of winter are superposed. The largest azimuth deviations correspond to thermospheric phases.

have relatively small deviations, generally less than 2°. The largest azimuth deviations come from the Itb phases, which turn at the highest levels of the atmosphere. For example, at 9 h the winds above 140 km flow towards the west, thus making eastward-propagating waves turn at a higher level (Fig. 7). The meridional winds are the strongest at this level, and thus significantly deflect the rays in a direction perpendicular to the ray direction. In addition, at the turning point the rays are propagating close to the horizontal, and thus spend the most time in the upper layers where they are most vulnerable to being deflected by the wind. Thus, the largest deviations are associated high-altitude turning points and with conditions of extreme winds. However, such far-reaching rays will be severely attenuated, and may not be easily detected by ground-based sensors.

Geomagnetic storms alter the turning heights and the azimuth deviations associated with a specific ray parameter (Fig. 7). At 3 h and 6 h the turning heights are reduced for It phases, and thus the azimuth deviations are smaller. However, at 18 h and 21 h turning heights are increased and the deviations also increase. Thus traveltimes and azimuth deviations depend on the magnitude and phase relationship of tide-induced and geomagnetic-induced winds.

We next launch 50 rays towards the west in order to compare downstream and upstream propagation with respect to the stratospheric winds. Traveltime as a function of range and time of day for the season of winter is shown in Fig. 10. Turning height as a function of slowness, winter day number and time of day is shown in Fig. 11. For propagation towards the west, against the predominant stratospheric winds, there are no predicted stratospheric arrivals. However, high slowness values usually associated with stratospheric reflections may be incorrectly ascribed to stratospheric ducted phases, whereas they may be refracted in the thermosphere. Fig. 11 shows that all the rays are reflected back in the thermosphere, principally at the two levels near 120 and 150 km. However, at 9, 12, 18, 21, and 0 h local time, a third thermospheric refraction level appears just below 100 km. This third waveguide is strongly affected by the geomagnetic index, as can be seen at 21 h in Fig. 11. The number of rays (and thus the amount of energy) that are trapped in this lower thermospheric waveguide is proportional to the AP index, or the amount of geomagnetically induced variability. This waveguide is enhanced at 18 h because at this time the zonal winds are predominantly towards the west and in phase with the geomagnetic-induced wind component and thus are sensitive to perturbations in the geomagnetic activity. These times and reflection heights correspond to maximum microbarom amplitudes at 11 and 22 h local time observed by Donn & Rind (1971) during a time of intensifying solar activity (solar maximum occurred in 1969). The increase in microbarom amplitudes was attributed to a reduction in reflection height, which would correspond to less acoustic attenuation. Our results suggest that their observations may be due to a combination of tidal effects and either geomagnetic effects or other mechanisms that may act in phase with the tidal winds to depress the reflection levels.

Fig. 12 shows the azimuth deviations as a function of range and time of day for rays propagating towards the west in winter. The deviations are relatively small, generally less than 5°. However, note the diurnal variability induced by the tide.

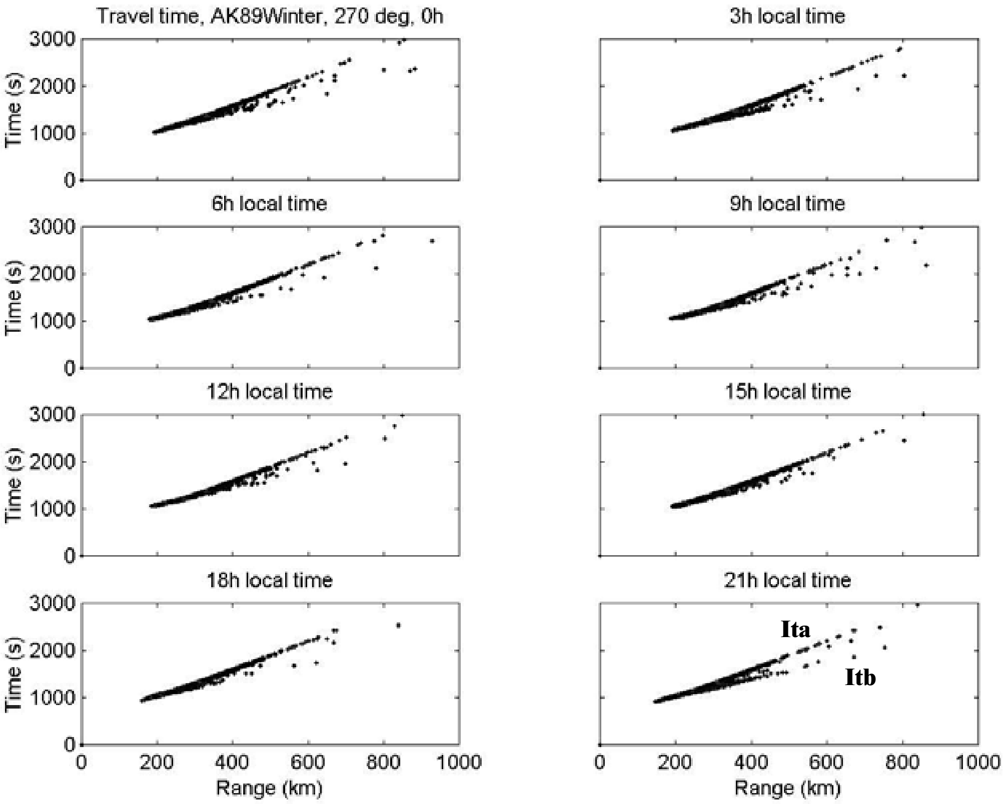

Figure 10. Traveltime curves for infrasonic waves propagating towards the west. All the traveltime curves for the season of winter are superposed. No stratospheric phases are predicted propagating upstream of the dominant stratospheric wind.

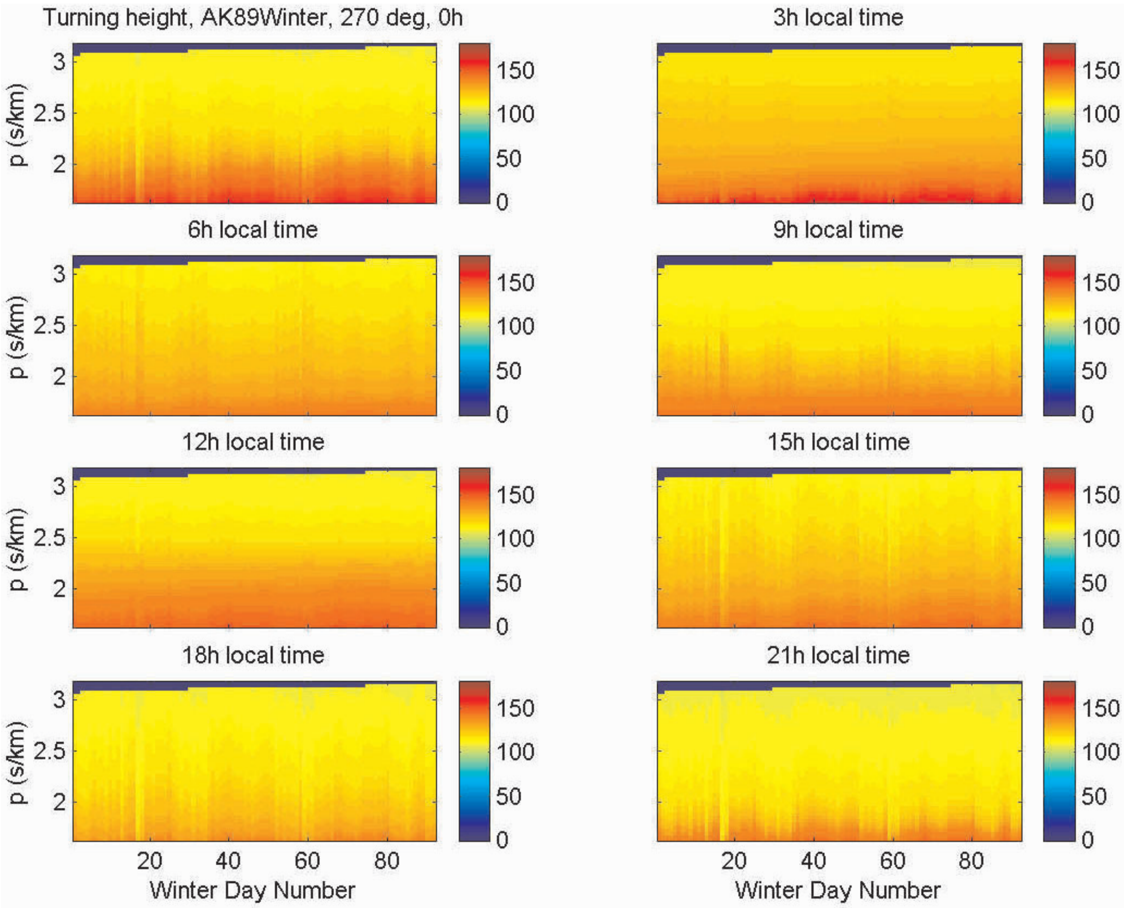

Figure 11. Turning heights for westward propagation as a function of slowness, local time and winter day number. As in Fig. 7, the height ranges corresponding to the two thermospheric phases depend on the tidal winds. There is an additional turning point just below 100 km.

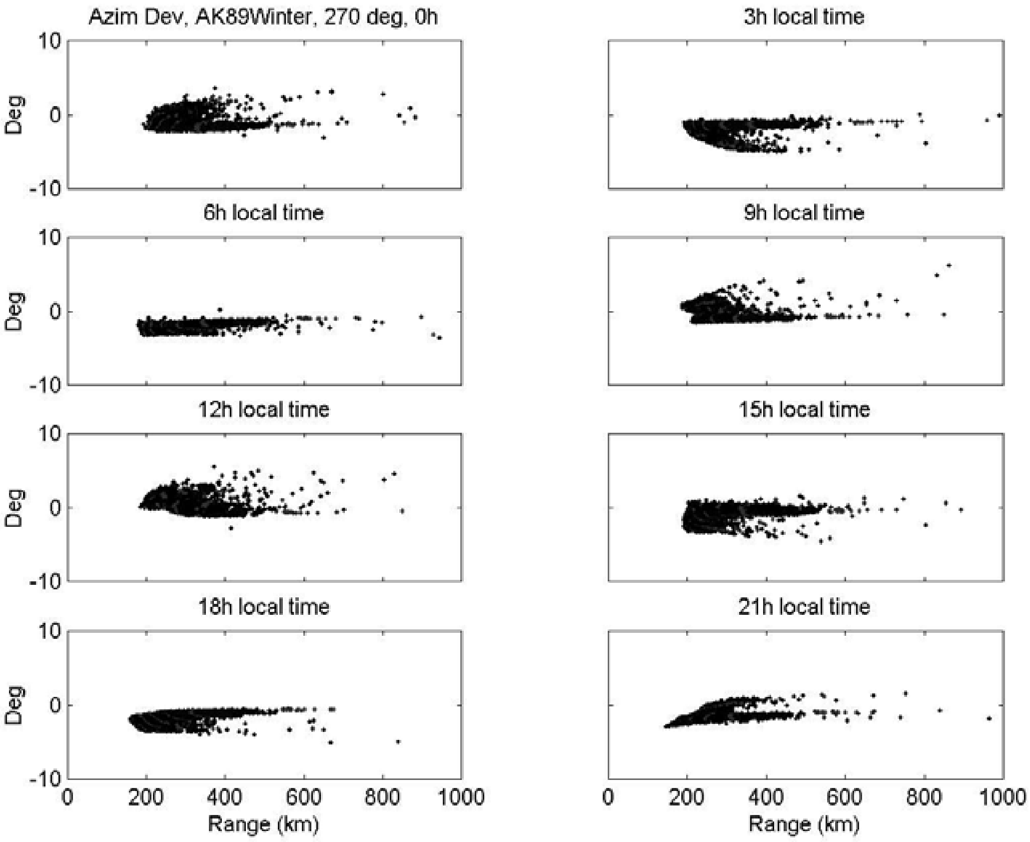

Figure 12. Azimuth deviation as a function of range and local hour for infrasonic waves propagating towards the west. All the azimuth deviations for the season of winter are superposed. As in Figs 8 and 9, the largest azimuth deviations correspond to thermospheric phases.

As in Fig. 8, the largest deviations correspond to the rays that are propagating higher in the atmosphere.

CONCLUDING REMARKS

The HWM and MSIS atmospheric models for Alaska during the season of winter 1989–90 were utilized to study the diurnal variability introduced by tidal and geomagnetic fluctuations on the traveltime curves, turning heights, and azimuth deviations of infrasonic waves propagating towards and against the dominant stratospheric winds. Significant diurnal variability can be attributed to the solar tides, whereas the AP index may affect both diurnal and daily changes. These are deterministic processes which may be either measured or predicted, and thus may be accounted for when trying to obtain accurate source locations from infrasonic signals.

According to our study, an arrival with a low apparent horizontal phase velocity may be either thermospheric or stratospheric. If the origin time and epicentre of a source are not known, the identification of a phase should be based on knowledge of the latest atmospheric conditions and determined by the waveguide height. Predicted azimuth deviations for the dominant phases (Is and Ita) are generally small, in agreement with historical data sets.

ACKNOWLEDGMENTS

This work was supported by DOE grant DE-FC04–98AL79801. Many thanks to Alexis LePichon for his editorial comments, which improved the manuscript. The authors are grateful to D. ReVelle and R. Whitaker, LANL, for their valuable discussions.

REFERENCES

Andrews, D.G., Holton, J.R. & Leovy, C.B., 1987. *Middle Atmosphere Dynamics,* Academic Press, San Diego.

Brown, D.J., 1999. Summary of infrasound source location meeting: San Diego, *November 9–10, 1998,* Center for Monitoring Research, Arlington.

Donn, W.L. & Rind, D., 1971. Natural infrasound as an atmospheric probe, *Geophys. J. R. Astr. Soc.,* **26,** 111–133.

Forbes, J.M., 1995. Tidal and Planetary Waves, *The Upper Mesosphere and Lower Thermosphere, AGU Monograph, 87,* eds Johnson, R. M. & Kileen, T. L., pp. 1–23, AGU Press, Washington DC.

Garcés, M., Hansen, R. & Lindquist, K., 1998. Traveltimes for infrasonic waves propagating in a stratified atmosphere, *Geophys. J. Int.,* **135,** 255–263.

Georges, T.M. & Beasley, W.H., 1977. Refraction of infrasound by upper-atmospheric winds, *J. acoust. Soc. Am.,* **61,** 28–34.

Hedin, A.E., 1991. Extension of the MSIS thermosphere model into the middle and lower atmosphere, *J. geophys. Res.,* **96,** 1159.

Hedin, A.E., *et al.*, 1996. Revised global model of upper thermospheric winds using satellite and ground-based observations, *J. geophys. Res.,* **96,** 7657–7688.

Hedin, A.E., Buonsanto, M.J., Cordrescu, M., Duboin, M.-L., Fesen, C.G., Hagan, M.E., Miller, K.L. & Sipler, D.P., 1994. Solar activity variations in midlatitude thermospheric meridional winds, *J. geophys. Res.,* **99,** 17601–17608.

Hitteregger, H.E., 1981. Representation of solar EUV fluxes for Aeronomical applications, *Adv. Space. Res.,* **1,** 39–42.

McKisic, J.M., 1997. *Infrasound and the Infrasonic Monitoring of Nuclear Explosions,* Department of Energy, Washington DC.

Procunier, R.W., 1971. Observations of Acoustic Aurora in the 1–16 Hz range, *Geophys. J. R. astr. Soc.,* **26,** 183–189.

Prolss, G.W., 1997. Ionospheric F-Region Storms, *Handbook of Atmospheric Physics,* Vol. II, ed Volland, H., Cambridge University Press, New York.

Rind, D. & Donn, W.L., 1975. Further use of natural infrasound as a continuous monitor of the upper atmosphere, *J. Atmos. Sci.,* **32,** 1964–1704.

Roble, R.G., 1995. Energetics of the Mesosphere and Thermosphere, *The Upper Mesosphere and Lower Thermosphere AGU Monograph, 87,* eds Johnson, R.M. & Kileen, T.L., pp. 67–88, AGU Press, Washington DC.

Salah, J.E., Deng, W. & Clark, R.R., 1996. Observed response of the earth's lower thermosphere to a major geomagnetic storm, *Geophys Res. Lett.,* **23,** 575–579.

Wilson, C., Olson, J. & Richards, R., 1996. *Library of Typical Infrasonic Signals*. ENSCO Inc, Melbourne, FL.